Polymer 49 (2008) 2444–2454

Contents lists available at ScienceDirect

Polymer

journal homepage: www.elsevier.com/locate/polymer

Towards the synthesis of high solids content waterborne poly(methyl methacrylate-*co*-butyl acrylate)/montmorillonite nanocomposites

Gabriela Diaconu, Maria Paulis, Jose R. Leiza*

Institute for Polymer Materials, POLYMAT, Departamento de Química Aplicada, Facultad de Ciencias Químicas, University of the Basque Country, Joxe Mari Korta zentroa, Tolosa Etorbidea 72, 20018 Donostia-San Sebastián, Spain

ARTICLE INFO

Article history:
Received 7 December 2007
Received in revised form 3 March 2008
Accepted 20 March 2008
Available online 28 March 2008

Keywords:
Emulsion polymerization
High solid latexes
Acrylic polymer/montmorillonite nanocomposites

ABSTRACT

Small angle X-ray scattering of Na-montmorillonite (Na-MMT) aqueous dispersions showed that at concentrations below 1.5 wt%, clay platelets were fully dispersed with an average distance between platelets higher than 16 nm. At higher concentrations (3 wt%) platelet–platelet interaction was not negligible and SAXS measurements detected ordered stack structures composed of 2–3 platelets with an average distance of around 14–16 nm. Thus, initiating an emulsion polymerization of methyl methacrylate and butyl acrylate in an aqueous phase containing Na-MMT at concentrations below 1.5 wt% allowed the production of stable and coagulum free waterborne nanocomposites having 30 wt% solids content, with exfoliated structure. The *in situ* produced poly(methyl methacrylate-*co*-butyl acrylate)/Na-MMT nanocomposite latexes provided better mechanical, thermal and permeability properties than composites prepared by blending pristine latex with Na-MMT or the pristine copolymer synthesized in the same conditions. Furthermore, for the first time nanocomposite latexes with 45 wt% solids content and intercalated morphologies having enhanced mechanical properties were also produced by seeded semibatch emulsion polymerization. The intercalated structure was likely due to the higher clay concentration in the aqueous phase that favoured platelet–platelet interaction, increased the viscosity of the polymeric dispersion and prevented a complete exfoliation.

1. Introduction

Synthetic polymer dispersions are mainly produced by emulsion polymerization. About half of these polymers are commercialized as waterborne dispersions. The main markets for these dispersions are paints and coatings (26%), paper and paper board coatings (23%), adhesive and sealants (22%) and carpet backing (9%) [1,2]. The technology available for the production of these products is mature (more than 50 years for most of the applications) and the room for improvement to cover the new demands of the market is limited. Certainly, there is still room for optimization of the existing plants to produce coatings and adhesives by emulsion polymerization, but the margin to create new and innovative materials based on the existing technology is limited.

A promising route to produce polymeric dispersions with unprecedented properties that can lead to new or significantly improved materials might come from the so-called nanocomposite materials. Polymer nanocomposites are hybrid materials composed in a large extent by a polymer matrix reinforced with a small volume fraction of nanoceramics or carbon nanotubes. These materials have attracted steadily growing interest due to their peculiar and unexpected properties as well as their unique applications in commercial sectors [3]. The incorporation of layered silicate clays (as sodium montmorillonite, Na-MMT) arranged on the nanometer scale with a high aspect ratio (or extremely large surface area) into polymer improves its mechanical performance significantly [4–6].

There are different routes to produce polymer nanocomposites that include: intercalation of polymer or pre-polymer from solution, melt intercalation and *in situ* polymerization. For the production of waterborne nanocomposites for coating and adhesive applications *in situ* emulsion polymerization is the best suited alternative, especially when hydrophilic pristine Na-MMT is employed. However, if organophilic clays (pristine clays where the naturally occurring cations have been substituted by means of cationic exchange with long alkyl ammonium salts) are employed, emulsion polymerization is not the best alternative [7–9] because the clay will not be incorporated into the polymer particles. A more reasonable technique will be miniemulsion polymerization if the clay can be encapsulated into the miniemulsion droplets for subsequent polymerization and production of the waterborne polymer/clay nanocomposite dispersions. We have recently shown that waterborne nanocomposites prepared with commercially modified montmorillonite

* Corresponding author. Tel.: +34 943015329; fax: +34 943017065.
E-mail address: jrleiza@ehu.es (J.R. Leiza).

0032-3861/$ – see front matter © 2008 Elsevier Ltd. All rights reserved.
doi:10.1016/j.polymer.2008.03.038

by miniemulsion polymerization significantly improved mechanical, thermal and barrier properties [7,8].

In this work the emulsion polymerization route to synthesize waterborne nanocomposites for coating applications was explored. Emulsion polymerization has been the polymerization technique most extensively used for the production of waterborne polymer–clay nanocomposites probably because it has been claimed that complete dispersion (exfoliation) of sodium montmorillonite clay (Na-MMT) in water is achieved. The structure of Na-MMT dispersed in aqueous phase has been studied in detail in this work by means of small angle X-ray scattering and is presented below. Lee et al. [10–13] were the first to exploit this feature and carried out emulsion polymerizations with several monomers including styrene, methyl methacrylate and acrylonitrile–styrene, producing in most of the cases intercalated nanocomposites upon film formation. The exfoliation of Na-MMT in the emulsion polymerization of MMA or MMA–BA was also claimed by some authors [14,15]. Other authors have also followed the emulsion polymerization technique, but using other surfactants and initiator systems (e.g. 2-acrylamido-2-methyl-1-propanesulfonic acid, AMPS [16,17]) to help compatibilize clay and polymer matrix and hence better dispersing the clay platelets in the polymer matrix in order to render nanocomposites with exfoliated structures [18–20].

Many works have used organically modified clays, O-MMTs, directly in emulsion polymerization processes by dispersing the hydrophobic clay in the aqueous phase [11,19,21–23]. First, the clay is rendered hydrophobic by exchanging the naturally occurring Na^+ and Ca^{2+} of the interlayer with long alkyl ammonium or phosphonium cations. In some cases clay aggregation (when dispersed in water) was avoided by addition of a peptizing agent, as it was shown by Negrete-Herrera et al. [24,25] for laponite modified with AIBA (2,2-azo-bis(2-methylpropionamidine) hydrochloride). In other processes, the modified clays were dissolved in the monomer, which was polymerized in a conventional emulsion polymerization procedure [26–28]. In this case, the organophilic clay cannot be incorporated into the polymer particles because diffusion through the water phase is not favoured, as it occurred with highly hydrophobic monomers that hardly polymerize in emulsion polymerization [29].

Other works [30,31] have also shown that it is possible to synthesize waterborne nanocomposites using clay platelets as the only stabilizing agent, the so-called pickering emulsions. However, the stability of these dispersions is very weak and they are very sensitive to the type of initiators employed during the polymerization.

In most of these works, formulations with low solids contents (<20%) and batch operation were used to produce the nanocomposites. These solid contents are far from what is required for commercial applications (>45%). Furthermore, to produce latexes with high solids content at industrial scale, a semicontinuous operation should be used to allow safe and efficient reactor temperature control.

The goal of this work was to produce high solids content waterborne acrylic/clay nanocomposites by emulsion polymerization using pristine Na-MMT. All acrylic monomer formulations are typically employed as binders for coating and paint formulations among other more specialized materials. First, the experimental and characterization procedures are briefly described. Second, the small angle X-ray scattering of Na-MMT aqueous dispersions is discussed. These measurements shed light on the effect of the concentration of Na-MMT in the morphology of the nanostructures produced. Then, polymerization kinetics and the properties of the nanocomposite latexes are introduced for latexes synthesized with 30 wt% solids content. Third, the morphological properties of the nanocomposite films are discussed. Mechanical, thermal and permeation properties of the waterborne nanocomposite films are presented and compared to the pristine copolymer latex prepared under the same conditions, and to a composite latex prepared by blending pristine latex and Na-MMT clay. Finally, we address the challenging issue of increasing the solids content of the formulations to produce acrylic/Na-MMT waterborne nanocomposites for coating applications. An operation strategy that allows the production of nanocomposite latexes with 45 wt% solids content and 3 wt% of Na-MMT will be presented.

2. Experimental section

2.1. Materials

Na-montmorillonite (Na-MMT) was provided by Southern Clay Products Inc. (Texas/USA) with a cationic exchange capacity (CEC) of 92.6 mequiv/100 g clay. The XRD analysis showed an interlayer space of 1.15 nm. The monomers: methyl methacrylate (MMA, Quimidroga) and butyl acrylate (BA, Quimidroga) were used without further purification. Sodium lauryl sulfate (SLS) and potassium persulfate (KPS) were purchased from Aldrich and used as received.

2.2. Preparation of the poly(methyl methacrylate-co-butyl acrylate)/MMT nanocomposites

Waterborne poly(methyl methacrylate-*co*-butyl acrylate)/MMT nanocomposite latexes with 3 wt% Na-MMT based on monomers were synthesized by seeded semibatch emulsion polymerization. All the reactions were carried out in a 1 L stirred tank glass reactor equipped with a jacket, reflux condenser, sampling device, nitrogen inlet, two feeding inlets and a stainless steel anchor stirrer equipped with two blade impellers rotating at 250 rpm. Reactor temperature, monomer and initiator feed flow rates were controlled by an automatic control system (Camile TG, Biotage). Waterborne nanocomposites with 30 and 45 wt% solids content were produced.

The formulation used for the preparation of nanocomposites with 30 wt% solids content by seeded semibatch emulsion polymerization is shown in Table 1. The typical procedure for the synthesis of these nanocomposite latexes was as follow: the seed with 20 wt% solids content (different MMA/BA co-monomer ratios were used) was synthesized batchwise at 75 °C for 1 h. All the Na-MMT was charged in the seed preparation. The remaining amount of co-monomers and an aqueous solution of KPS were fed continuously into the reactor in two different streams for 3 h. Afterwards, the reactor content was allowed to polymerize for one more hour at 75 °C. The final solids content of the latex was 30 wt% and the content of Na-MMT was 3 wt% based on monomer. For the sake of comparison, a blank emulsion latex was synthesized following the above described synthesis procedure, but without Na-MMT. Furthermore, a nanocomposite latex was also prepared by blending the blank emulsion latex with Na-MMT (3 wt% based on the

Table 1
Formulation used for the seeded semibatch emulsion copolymerization of MMA/BA in the presence of Na-MMT

Reagent	Seed[a]	Feeding streams[b]	
	Initial charge	F1	F2
MMA (g)	$(135 \times X_{MMA})$	$(135 \times (1 - X_{MMA}))$	–
BA (g)	$(135 \times X_{BA})$	$(135 \times (1 - X_{BA}))$	–
SLS (g)	5.4	–	–
Na-MMT (g)	8.1	–	–
KPS (g)	0.675	–	0.675
H_2O (g)	550	–	30

X_{MMA} and X_{BA} are the MMA and BA weight fractions, $X_{MMA} + X_{BA} = 1$. Solids content: 30 wt%.

[a] Seed prepared in batch, at 75 °C for 1 h.

[b] Feeding time 3 h.

polymer of the blank latex) by magnetic stirring (700 rpm) for 3 h at room temperature.

Table 2 shows the formulation used for the synthesis of the waterborne nanocomposite latex with 45 wt% solids content. For the preparation of the 45 wt% solids content waterborne nanocomposite latexes a similar procedure as that described above was used. In this case the solids content of the seed was 25 wt%. The amount of Na-MMT required to produce the nanocomposite latex (3 wt% based on monomer) was split between the seed and the monomer pre-emulsion feed.

Table 3 presents the summary of the experiments carried out to produce waterborne acrylic polymer/clay nanocomposite latexes. Note that the final co-monomer ratio was MMA/BA = 50/50 wt% for all the reactions.

2.3. Characterization and measurements

Polymer particle size was measured by dynamic light scattering (DLS) using a Coulter N4 plus in unimodal analysis. For this analysis, a fraction of the latex was diluted with deionized water. The reported particle size values represent an average of three repeated measurements. Particle size distribution of the final latexes was measured by means of a disc centrifuge photosedimentometer (Brookhaven BI-DCP). Conversion was measured by gravimetric analysis.

The gel contents of the samples were measured via conventional Soxhlet extraction, using tetrahydrofuran (THF) as solvent. A glass fiber disk was impregnated with a few drops of latex and the extraction was carried out for 24 h under reflux conditions at about 80 °C. The gel remained in the glass fiber, whereas the polymer soluble fraction was recovered from THF solution. The amount of gel was calculated using the following equation:

$$\text{gel}\ (\%) = \frac{w_{\text{gel}} - (w_{\text{total}} x_{\text{clay}})}{w_{\text{total}} - (w_{\text{total}} x_{\text{clay}})} \times 100$$

where w_{gel} is the amount of insoluble polymer that remained in the glass fiber, w_{total} is the whole polymer sample and x_{clay} is the fraction of clay content based on monomer in the formulation.

The molecular weight distribution and the average molecular weights ($\overline{M}_{\text{w}}$) of the soluble polymer fraction were determined by gel permeation chromatography using a size exclusion chromatograph (SEC) instrument that consists of a pump (Waters 510), three columns (Styragel HR2, HR4 and HR6) and a differential refractometer (Waters 2410) as detector. The soluble polymer fraction obtained by Soxhlet extraction was concentrated, filtered (filter pore size 0.45 μm, Albert) and then injected into the SEC. Polystyrene standards were used to calibrate the equipment and the absolute molecular weights were calculated using the Mark–Houwink–Sakurada constants ($k_{\text{MMA}} = 14.3 \times 10^{-5}$ dl/g, $\alpha_{\text{MMA}} = 0.71$ and $k_{\text{BA}} = 12.3 \times 10^{-5}$ dl/g, $\alpha_{\text{BA}} = 0.7$).

Wide angle X-ray diffraction (WAXD) analyses were performed on a Philips PW 1729 Generator connected to a PW 1820 (Cu Kα radiation with $\lambda = 0.154056$ nm) at room temperature. The range of the diffraction angle was $2\theta = 2$–12° with a scanning rate of 0.02°/3 s. The (001) basal spacing of the clay (d) was calculated using the Bragg equation: $n\lambda = 2d \sin\theta$, where λ is the wavelength of the X-ray and θ is the scattering half angle. To perform the WAXD analysis, films cast from the latex were thoroughly rinsed to get rid of the SLS and to avoid its peaks at 2.5°, 5° and 7° in the WAXD patterns.

Small angle X-ray scattering (SAXS) experiments were carried out on the SAXS instrument constructed at the European Synchrotron Radiation Facility (ESRF) in Grenoble (France), using the Synchrotron Radiation of the beamline BM16. The beamline is equipped with a 2048 × 2048 (2 × 2 binned) pixels position-sensitive two-dimensional marCCD detector with an active surface area of 165 mm in diameter. The measurements were done using a monochromatic X-ray at $\lambda = 0.726$ nm wavelength (energy $E = 17.068$ keV) and at a sample-to-detector distance of 3.93 m. The samples were calibrated to the diffraction peaks of silver-behenate.

Dynamic mechanical thermal analysis (DMTA) was used to analyze the relaxation behavior of the polymer/clay nanocomposites. To perform the DMTA analysis a film of 1 mm thick was heated from −50 °C to 100 °C with a heating rate of 0.3°/min. The thermal stability of the nanocomposites was studied using thermogravimetric analysis (TGA). To perform the TGA analysis, the sample (10 mg) was heated from 20 °C to 600 °C with a heating rate of 10°/min using a TA Instrument Thermogravimetric Analyzer model Q500. The stress–strain behavior of the nanocomposites was determined in a universal testing machine, INSTRON 4301, operated with a crosshead speed of 20 mm/min. The tests were carried out at 23 °C and 50% relative humidity.

The barrier properties were investigated by measuring the water vapor permeation. The latex film was placed in the upper part of a cell filled with a certain amount of water. The cell was well-sealed so that water only could escape by permeating through the film. The water vapor transfer rate (WVTR, g mm/cm^2 days) was calculated with the following equation [32]:

$$\text{WVTR} = 8.64 \times 10^5 \frac{Bl}{A(1 - a_{\text{ext}})}$$

where B is slope of the water vapor loss in time (g/s), l is the thickness of the latex film (mm), A is the area of the latex film ($A = 2.54$ cm^2), and a_{ext} is water vapor activity (measured using a thermohygrometer). The measurements were carried out in a temperature-controlled chamber at 30 °C and the weight loss of the water vapor was recorded every 15 s for 4 h.

Table 2
Formulation used for the seeded semibatch emulsion copolymerization of MMA/BA in the presence of Na-MMT

Ingredient	Seed[a]	Feeding streams[b]	
	Initial charge	F1	F2
MMA (g)	40	162.5	–
BA (g)	40	162.5	–
Na-MMT (g)	2.4	9.75	–
SLS(g) (g)	2	8.125	–
H_2O (g)	250	220	25
KPS (g)	0.4	–	1.625

Solids content: 45 wt%.
[a] Seed prepared in batch, at 75 °C for 1 h.
[b] Feeding time 3 h.

Table 3
Summary of the nanocomposite latexes synthesized by seeded semibatch emulsion polymerization

Sample	Co-monomer ratio MMA/BA		Clay content (%)	Solids content (%)
	Seed stage	Feeding stage		
EP1	50/50	50/50	0	30
EP2	50/50	50/50	3	30
EP3	Physical blend (EP1 + 3%Na-MMT)		3	30
EP4	100/0	0/100	3	30
EP5	80/20	20/80	3	30
EP6	50/50	50/50	3	45

3. Results and discussion

3.1. SAXS analysis of Na-montmorillonite aqueous dispersions

A dry montmorillonite powder swells spontaneously when contacted with water [33]. The dry clay usually imbibes water and becomes a gel, and it can be stirred up with more water to yield a suspension or sol. Small angle X-ray scattering (SAXS) is a technique used to determine the internal and external structure of

colloidal particles over a wide range of length scales [34]. The colloidal behavior of synthetic (laponite clay [25,35]) and natural clay (Na-montmorillonite clay [36–38]) has been studied using SAXS technique. In this study various Na-MMT aqueous dispersions were analyzed by the small angle X-ray scattering (SAXS) technique. Fig. 1 presents the scattering profiles of 1–4% Na-MMT aqueous dispersions. The scattering intensity, $I(q)$, decayed with increasing the scattering vector, q, this behavior being typical of thin-layer particles. It can also be noticed that increasing the clay content, the scattering intensity increased. The absence of peaks in the SAXS profiles indicated that the clay was swollen with water and that the preferential agglomeration of platelets in stacks was lost when being dispersed in water.

This kind of intensity profiles have been used to extract data of a single layer width (T) from the Guinier approximation at low scattering vectors (low q) [34]. However, as Shang et al. demonstrated, this approximation can only be used when no interaction between single platelets occurs in the aqueous dispersion, which occurs only at clay concentrations below 0.4% in water [36,37]. Therefore, Guinier's approximation cannot be applied to the data obtained in the present study.

Saunders et al. [35] calculated an experimental structure factor for concentrated dispersions, $S(q)$, by dividing the measured intensity for the concentrated dispersion, $I(q)_{\mathrm{conc}}$, by the intensity obtained for a diluted dispersion, $I(q)_{\mathrm{dil}}$ of the same type of particles (Eq. (1)) [35].

$$S(q) = \frac{I(q)_{\mathrm{conc}}\phi_{\mathrm{dil}}}{I(q)_{\mathrm{dil}}\phi_{\mathrm{conc}}} \quad (1)$$

where ϕ_{dil} and ϕ_{conc} are the particle volume fractions in the diluted and concentrated dispersions, respectively. Taking into account that no interaction between particles takes place in the diluted systems, peaks in the structure factor will arise from interactions between particles in the concentrated system. Fig. 2 presents the $S(q)$ plots for 1.5, 3 and 4% Na-MMT dispersions in water, taking the intensity given by the 1% Na-MMT dispersion as the one of the diluted dispersion.

As it can be seen, while no peak appeared in the 1.5% Na-MMT dispersion, a peak appeared both in the 3% and 4% Na-MMT dispersions. The presence of peaks was attributed to the existence of platelets interacting face to face at a interlayer distance of d, where d could be calculated from the position of the peak ($q_{\max}$) by $d = 2\pi/q_{\max}$ [35]. The position of the peak for the 3% Na-MMT

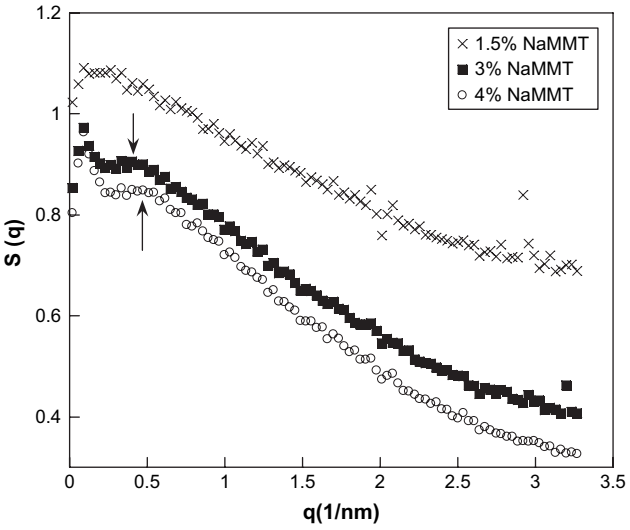

Fig. 2. $S(q)$ structure factor plots for Na-MMT aqueous dispersions with different clay contents.

dispersion was 0.4 nm^{-1}, which corresponded to a distance of 16 nm, while the position shifted to higher q for the 4% Na-MMT dispersion, to 0.46 nm^{-1}, corresponding to a distance of 14 nm.

It can be argued that the 1% Na-MMT dispersion was not diluted enough to consider it in the above mathematical treatment. Therefore the Porod plot analysis of the obtained intensity data was also performed. Fig. 3 presents the $I(q)\cdot q^2$ vs q plots for the different Na-MMT concentrations in water.

As it can be observed, no peak appeared again in the 1 and 1.5% Na-MMT dispersions in water, while the 3 and 4% dispersions presented a broad peak. In this case, the position of the peak for the 3% Na-MMT dispersion was 0.45 nm^{-1}, corresponding to a distance of 14 nm, while the position shifted to higher q for the 4% Na-MMT dispersion, to 0.53 nm^{-1}, which corresponded to a distance of 12 nm. Even if the values are 2 nm smaller than the ones obtained with the structure factor plots, it has been proven that a certain platelet aggregation occurs above 3% Na-MMT concentration in water. To know the amount of clay layers involved in this aggregation, Ciccariello and Sobry [39] proposed the following equation (Eq. (2)):

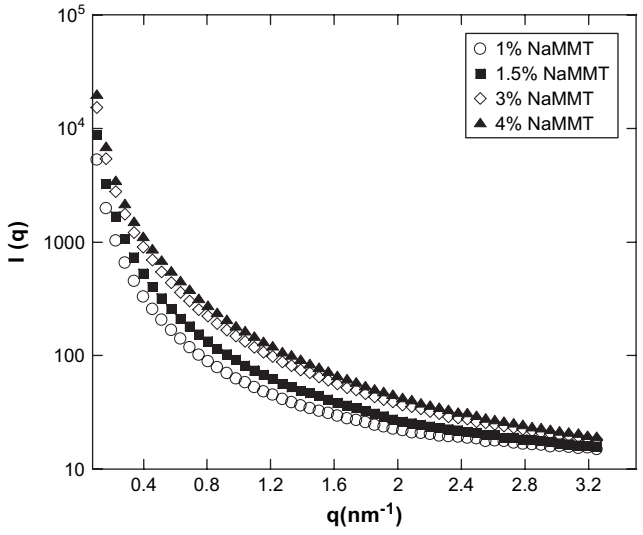

Fig. 1. Plots of $I(q)$ vs q for Na-MMT aqueous dispersions with different clay contents.

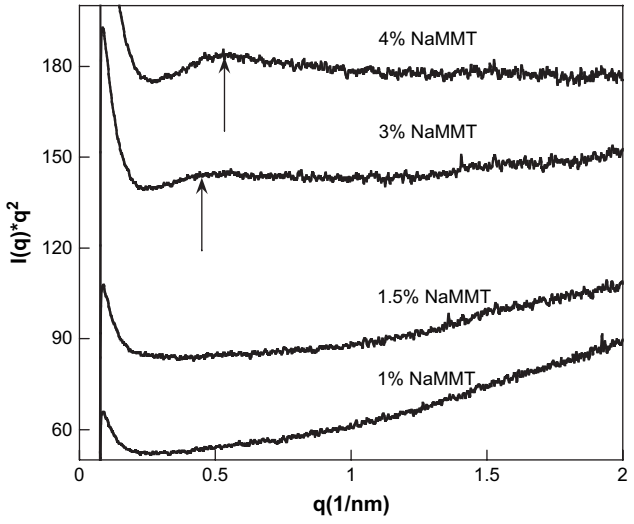

Fig. 3. $I(q)\cdot q^2$ vs q plots for Na-MMT aqueous dispersions with different clay contents.

$$I(q)\cdot q^2 \propto \frac{\sin^2(qt/2)\cdot\sin^2(Ndq/2)}{q^2\sin^2(qd/2)} \quad (2)$$

where N is the number of platelets in a stack, d the distance between them and t the thickness of the platelet (0.97 nm). If the distance obtained from the Porod plot for 4% Na-MMT concentration is used, model predictions for different N can be calculated, as plotted in Fig. 4. According to the model predictions the best fit was obtained for $N = 2$, which means that there are two platelets per stack.

If the average distance between layers in a completely dispersed-noninteracting clay dispersion is to be calculated, the equation proposed by Callaghan and Ottewill [40] can be used (Eq. (3)).

$$H_0 = \frac{2V_s}{m_{clay}A_s} \quad (3)$$

where H_0 is the maximum platelet separation, V_s is the solvent volume, m_{clay} is the mass of clay and A_s is the specific surface area of the montmorillonite (750 m^2/g) [33]. H_0 ranges from 270 nm for 1% Na-MMT dispersion to 67 nm for 4% Na-MMT dispersion, provided that platelet–platelet interaction is negligible. Therefore taking into account the aforementioned analysis, it can be said that clay dispersions of 1 and 1.5% Na-MMT, presented a completely exfoliated structure in water (with average distances at around 270–180 nm between platelets, respectively) and that above 3% Na-MMT in water, a certain number of platelets tend to interact, likely in pairs separated at distances of 14–16 nm (from the ideal 89 nm if they would be completely dispersed). When the clay concentration in water increased to 4%, the distance in the stack lowered to 12–14 nm, and the number of this aggregated stacks increased.

The important conclusion of this study is that the average distance between clay platelets is larger than 15 nm in Na-MMT aqueous dispersions with concentrations up to 3%. Therefore, if to an aqueous dispersion of clay, monomer, emulsifier and initiator are added, it might be possible to initiate the polymerization between the platelets. Either homogeneous nucleation or micellar nucleation (micelles can be located between clay platelets) might occur depending on the concentration of emulsifier employed and the aqueous solubility of the co-monomers used in the polymerization. Some authors [41] also argued that polymerization can be initiated in the individual clay platelets. Therefore, emulsion polymerization seems to be well suited to produce exfoliated waterborne polymer/clay nanocomposites.

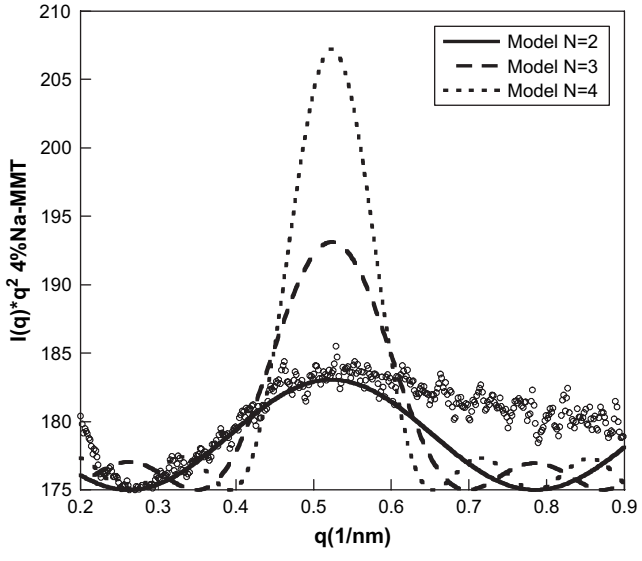

Fig. 4. Comparison between the experimental $I(q)\cdot q^2$ vs q data for the 4% Na-MMT dispersion with the Ciccariello model predictions for different number of platelets per stack (N).

3.2. Polymerization kinetics

A series of experiments (EP1, EP2, EP4 and EP5) with final co-monomer composition MMA/BA = 50/50 wt% were carried out under seeded semibatch conditions with and without Na-MMT in the polymerization. The Na-MMT clay was loaded in the seed preparation stage and different co-monomer ratios were employed in this stage as described in Table 3. The remaining monomer was fed at constant flow rate for 3 h to render waterborne nanocomposite copolymers with 30 wt% solids content (MMA/BA = 50/50 wt%) and 3 wt% of clay. All the nanocomposite latexes were stable and presented no coagulum.

Fig. 5 presents the time evolution of the instantaneous conversion for these latexes with 30 wt% solids content. The instantaneous conversion is defined as the amount of polymer produced divided by the amount of monomers fed until the sampling time. As it can be seen, the evolution of the instantaneous conversion was not affected by the presence of the clay, and the processes evolved under rather starved conditions (above 92% in all cases). The evolution of the particle size along the reaction for runs EP1, EP2, EP4 and EP5 is shown in Fig. 6. The particle sizes of the seeds were the same for all the reactions except for latex EP4 (MMA/BA = 100/0, that is a homopolymerization of MMA) that was slightly higher. In the feeding stage, particle size increased with the conversion (feeding time) indicating that secondary nucleation did not take place during the monomer addition period. Chern et al. [41] in *ab initio* emulsion polymerizations of styrene in the presence of 1 wt% Na-MMT found that for high SDS concentration ([SDS] ≥ 13 mM) micellar nucleation predominated and for lower SDS concentration the contribution of the polymerization associated to Na-MMT increased significantly. In complete absence of micelles (2 mM) the clay contribution was of the same order as the one in absence of Na-MMT in the polymerization. They found that the particle sizes slightly decreased in the polymerization carried out in the presence of the Na-MMT and at the same [SDS], the polymerization rate was faster for the runs with Na-MMT. Contrary to that found by these authors, in this work the presence of the clay had little influence in the nucleation of the seed polymer particles, likely because of the high concentration of surfactant employed during the seed polymerization ([SLS] = 36 mM) and consequently on the subsequent polymerization in semibatch.

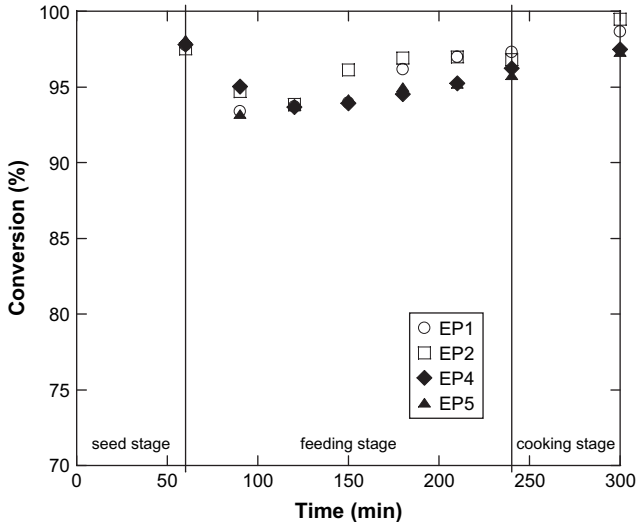

Fig. 5. Time evolution of conversion for runs EP1, EP2, EP4 and EP5.

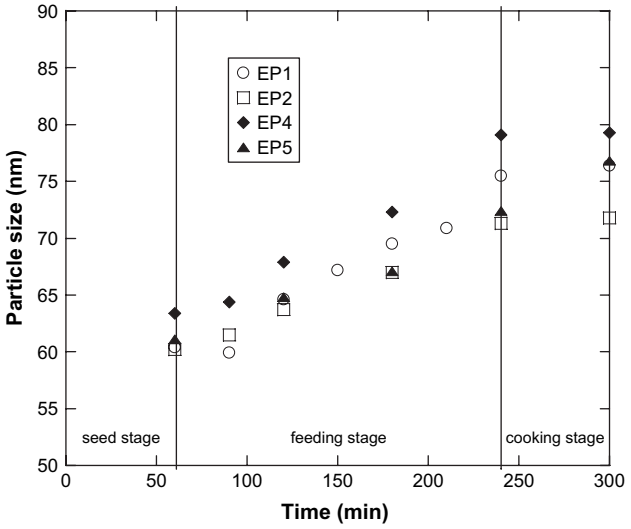

Fig. 6. Time evolution of particle size for runs EP1, EP2, EP4 and EP5.

The final particle size distributions for EP1, EP2, EP4 and EP5 runs are presented in Fig. 7. For run EP1 (blank emulsion latex) a unimodal and relatively narrow particle size distribution was obtained. For runs EP2, EP4 and EP5 the distributions were broader with a long tail with bigger particles, likely due to the presence of the clay. Assuming an average size of 160 nm for the clay, the average particle size of latex EP2 (72 nm) and the specific surface area of Na-MMT to be 750 m^2/g, the ratio between the number of particles and the number of completely exfoliated platelets is roughly 6, which means that at most 14% of the platelets can be associated somehow with the polymer particles. Therefore it is not surprising that the average particle diameter is lower than 100 nm for the polymer/clay nanocomposites.

3.3. Gel content and molecular weight distribution

Table 4 lists the gel content, average molecular weight and polydispersity index for EP1–EP5 latexes obtained by Soxhlet extraction and size exclusion chromatography. The gel content for EP1, EP2 and EP4 was negligible, however, in the case of EP5 run where the co-monomer ratio in the seed was MMA/BA = 80/20 wt%, the gel content increased to 6.2. This can be explained as

Table 4
The M_w, PDI and gel content of runs EP1–EP5

Sample	M_w (g/mol)	PDI (M_w/M_n)	Gel content (%)
EP1	1.08×10^6	10.9	<1
EP2	8.93×10^5	12.2	<1
EP4	1.60×10^6	1.8	<1
EP5	1.38×10^6	1.9	6.2

M_w is the weight average molecular weight.

follows: the seed contained negligible gel in all the cases because polymerizations were carried out in batch (polymer concentration in particles is only high at the very end of the process and hence chain transfer to polymer is not important [42,43]), the important amount of MMA employed that reduced labile H sites in the backbone, and the lower activity towards H abstraction of MMA terminated radicals [44,45]. During the semibatch period, latexes EP1, EP2 and EP4 did not produce any gel either. For latexes with 50/50 wt% composition in the seed and in the feeding this is in good agreement with other works [44–46] and can be mainly attributed to the lower activity of MMA terminated radicals that are predominant during the whole feeding period. However, one might expect that for latexes EP4 and EP5, where pure BA and 80 wt% rich BA streams were fed, some gel polymer might be formed. Certainly, for EP4 the seed polymer did not contain any labile H and hence although instantaneous conversion was high and only BA radicals were present, a negligible amount of gel polymer was formed. Nevertheless $\overline{M}_w$ for runs EP4 and EP5 were higher than for EP1 and EP2, indicating that chain transfer to polymer was more important in this case. For nanocomposite latex EP5, the gel fraction was low, but not negligible. This result indicates that the presence of some labile H in the seed polymer (20 wt% of BA) was enough to allow chain transfer to polymer to occur from the beginning of the feeding stage, and hence some gel was formed.

3.4. Morphology of the nanocomposites

The morphology of the nanocomposites was analyzed from two points of view. On one side the morphology of the latex was analyzed by small angle X-ray scattering (SAXS) and on the other hand, the morphology of the dried films obtained from the latex was analyzed by wide angle X-ray diffraction (WAXD).

Fig. 8 presents the SAXS patterns for latex EP1 and EP2 measured in their liquid form. As it can be seen, fringes typical of spherical particles [47] appear in both patterns, even if they are

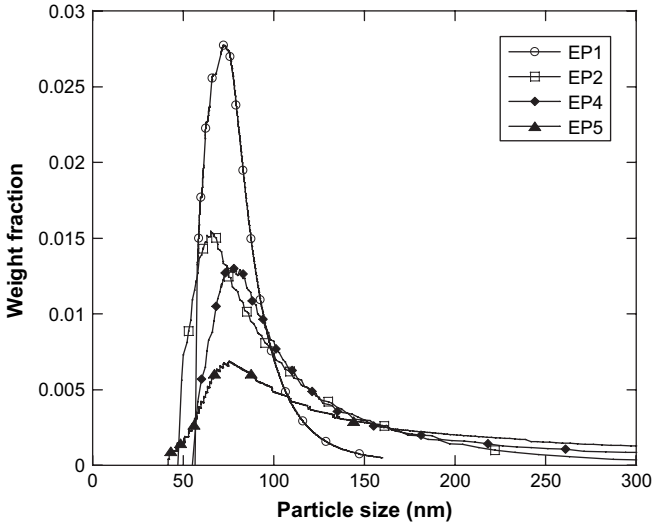

Fig. 7. Final particle size distributions measured by DCP for runs EP1, EP2, EP4 and EP5.

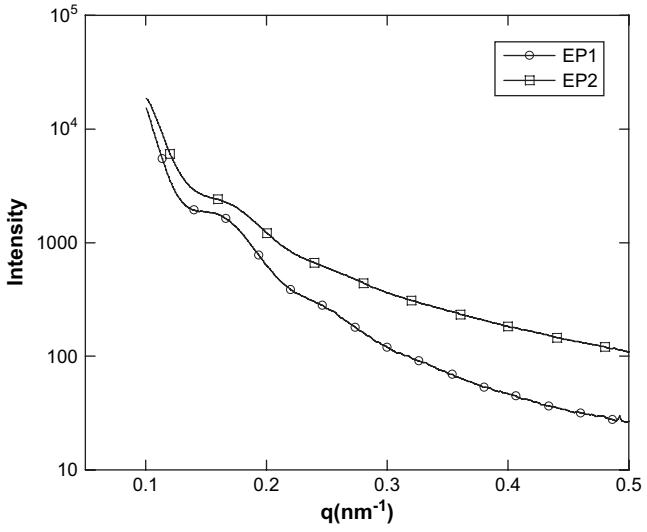

Fig. 8. SAXS patterns of EP1 and EP2 latexes.

somehow attenuated for latex EP2 containing clay. In a recent publication we have shown SAXS patterns of blank latexes and polymer/clay nanocomposite latexes prepared by miniemulsion polymerization [8]. In that case organophilic Cloisite 30B clay was used, instead of hydrophilic Na-MMT. The miniemulsion latex without Cloisite 30B presented clear fringes, while the latex with Cloisite 30B had almost no fringes. The disappearance of the fringes in that case was explained by the attachment of the more hydrophobic clay platelets to the surface of particles, losing their sphericity and the scattering observed mimicking that of disc-like structures. The results obtained for the latexes prepared by emulsion polymerization with Na-MMT suggest that the scattering of spherical particles is still dominant in the SAXS pattern, which might indicate that the clay platelets are preferentially located in the aqueous phase.

The nanocomposites were also analyzed by wide angle X-ray diffraction (WAXD) to obtain the structure of the clay in the polymer matrix after casting films from the latex. WAXD patterns were measured for the seed latex films (note that clay was totally loaded during seed preparation) and the final latex films for nanocomposites EP2, EP4 and EP5. Latex EP3 prepared by blending was also analyzed and all the results are shown in Fig. 9. The characteristic peak of the Na-MMT powder clay appears at $2\theta = 7.63^\circ$ which corresponds to an interlayer space of $d = 1.15$ nm. The film made out of the seed of run EP4 (with co-monomer ratio MMA/BA = 100/0 wt%) shows no peak in the WAXD pattern indicating that PMMA/Na-MMT nanocomposite with exfoliated structure was obtained. This is in agreement with the results presented by Yeom and Kim [48]. The films made out of the seeds of runs EP2 (with co-monomer ratio MMA/BA = 50/50 wt%) and EP5 (with co-monomer ratio MMA/BA = 80/20 wt%) did not show any peak either (the peaks in the patterns of EP2 were due to SLS) indicating also an exfoliated structure of the clay in the seed stage. The WAXD patterns of final latex films are shown in Fig. 9b. It can be seen that diffraction peaks are not present for runs EP2, EP4 and EP5 indicating that exfoliated nanostructures were also obtained in the final latex at least from the WAXD analysis. However, a peak at $2\theta = 6.0^\circ$ appears in the case of composite EP3 indicating the presence of Na-MMT platelet stacks with an interlayer space of $d = 1.47$ nm.

It is well known that transmission electron microscopy (TEM) can provide useful information in a localized area concerning the morphology, structure and spatial distribution of the dispersed phase of the nanocomposites. Thus XRD and TEM techniques are regarded as complementary to each other for the characterization of the polymer/clay nanocomposites [3]. Fig. 10 shows the TEM micrographs for nanocomposite films EP2 and EP3, where the darker part represents the clay and the lighter part the polymer. For nanocomposite EP2, individual layers dispersed in the polymer matrix can be observed and also zones with more than one clay layer well distributed into the polymer matrix (these zones represent the intercalated structures) can be distinguished. Thus the TEM micrograph confirms that a mixture of intercalated and exfoliated structure was obtained for nanocomposite EP2 which is in agreement with the WAXD pattern.

For composite EP3 it can be observed that the clay is not well dispersed in the polymer matrix and tactoids and stacks of clay platelets (the dark zones), as well as some intercalated structures can be observed (see Fig. 10b), as shown by the WAXD analysis.

The XRD and TEM results indicate that partially exfoliated poly(methyl methacrylate-*co*-butyl acrylate)/MMT nanocomposites have been successfully obtained by seeded semicontinuous emulsion polymerization when the clay was incorporated *in situ* during the polymerization reaction (runs EP2, EP4 and EP5) whereas aggregates of clay platelets, and hence a poor dispersion of the clay in the polymer matrix, were observed in the nanocomposite obtained by physical blend (run EP3).

3.5. Mechanical, thermal and barrier properties of nanocomposites

End-use properties of the films cast from the waterborne nanocomposite latexes were measured using the techniques discussed in the characterization section. Table 5 presents a summary of the mechanical, thermal and barrier properties measured to the blank emulsion latex (EP1), the *in situ* synthesized waterborne nanocomposite (EP2) and the waterborne composite prepared by physical blend (EP3). Additional information of these measurements is included as Supplementary data.

The nanocomposites EP2 and EP3 exhibit higher tensile strength compared to the pure copolymer, EP1. The increment of the tensile strength can be explained by the increase of the toughness of the nanocomposites caused by the presence of intercalated polymer chains in the interlayer space of clay. This increase is done at the expense of a reduction in the elongation at break that was significantly more affected in the blend composite EP3. This is in agreement with the morphology of the nanocomposite observed in both XRD and TEM analysis, where more tactoids and a worse dispersion of the clay was observed for latex EP3, that was produced by

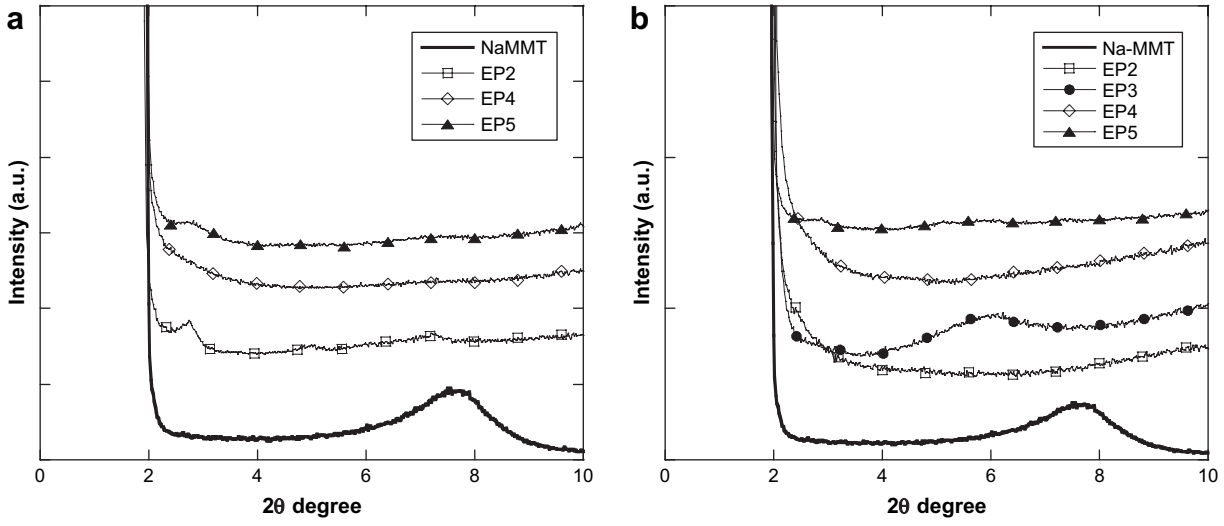

Fig. 9. WAXD patterns of Na-MMT powder clay and nanocomposites EP2–EP5: (a) after seed stage latex films, and (b) final latex films.

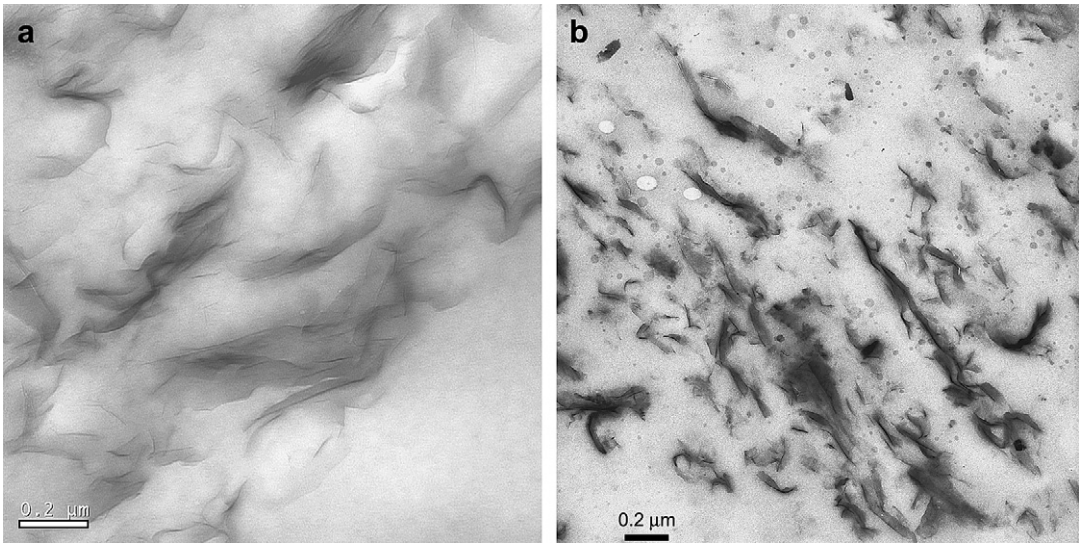

Fig. 10. TEM micrographs of nanocomposite EP2 (a) and composite EP3 (b).

Table 5
Mechanical, thermal and barrier properties of the waterborne nanocomposites

Sample	Tensile strength[a] (MPa)	Elongation at break[a] (%)	Storage modulus[b] (GPa)		T_g[b] (°C)	T_d[c] (°C)		WVTR[d] (g mm/cm^2 days)	
			50 °C	75 °C		10 wt% loss	50 wt% loss	As prepared	Washed film
EP1	9 ± 1	326 ± 58	1.95	0.83	38.3	348	383	26.0 ± 1.3	21.0 ± 0.3
EP2	13 ± 0.5	270 ± 18	14.4	9.55	39.5	358	395	13.6 ± 0.2	11.8 ± 0.2
EP3	15 ± 0.5	152 ± 9	19.0	8.91	42.0	351	391	13.7 ± 0.5	12.3 ± 0.7
EP6	13 ± 2	269 ± 15	8.91	3.54	40			N/A	N/A

[a] Stress–strain analysis in an INSTRON 4301 machine.
[b] Dynamic mechanical thermal analysis, DMTA.
[c] Thermal gravimetric analysis, TGA.
[d] Water vapor transmission rate.

a blending procedure. In this sense, Beall and Tsipursky [49] concluded that unexfoliated platelets can act as stress concentrators, contributing to a decrease in the elongation at break. Hence, the poor dispersion of the clay in the polymer matrix determined the strong decrease of the elongation at break for composite EP3 compared to the pure copolymer EP1 and the nanocomposite prepared by *in situ* emulsion polymerization, EP2.

It can be noticed that at temperatures above T_g, the storage modulus of the nanocomposites EP2 and EP3 was higher than the storage modulus of the pure copolymer EP1, in agreement with other works [16,17,23]. Above T_g, when the material becomes soft, the reinforcement effect of the clay is prominent due to the restricted movement of polymer chains surrounding the clay platelets.

Glass transition temperature, T_g, also increased for the nanocomposites EP2 and EP3, but the increase was modest (less that 4 °C) and especially for EP2 where the increase was roughly only one degree (see Table 5). This is important for latexes in coating applications because an increase in the T_g might affect the film formation temperature in a deleterious way.

On the other hand, the decomposition temperature of the nanocomposites increased with respect to the pure copolymer and the increase was higher for the *in situ* synthesized nanocomposite, EP2. Both the onset decomposition temperature (measured at 10 wt% loss) and the 50 wt% loss were improved in the nanocomposites. Many researchers believe that the role of clay in the nanocomposite structure might be the main reason for the difference in TGA results. The clay acts as a heat barrier, which could enhance the overall thermal stability of the system [50]. Thereby, in the initial stage of thermal decomposition, the clay could shift the decomposition temperature to higher values. However, after that, the stacked clay layers could hold accumulated heat that could be used as a heat source to accelerate the decomposition process.

Water vapor permeability, WVTR, was also studied for the pure copolymer, EP1 and the nanocomposites EP2 and EP3. The data shown in Table 5 correspond to the film–air interface. In all the cases the WVTR decreased when the latex film was rinsed with distilled

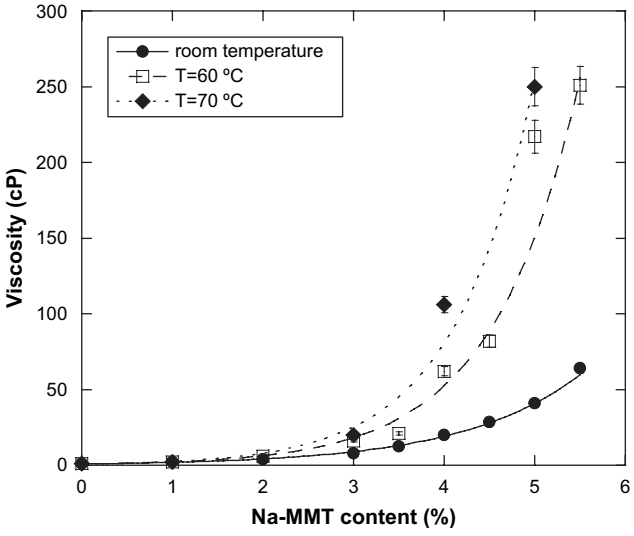

Fig. 11. Viscosity of Na-MMT aqueous dispersions at different Na-MMT content and temperatures.

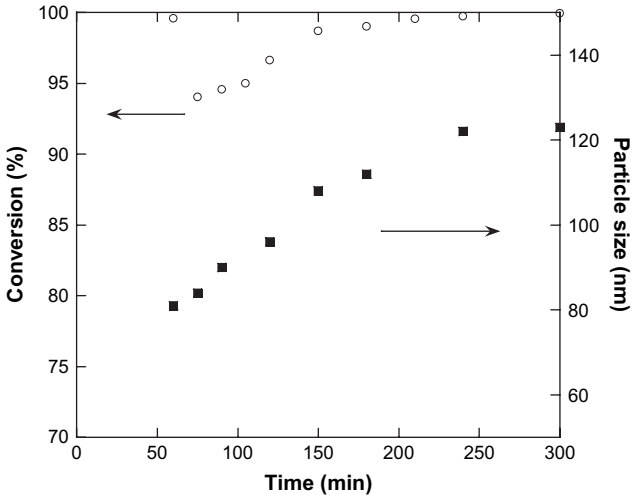

Fig. 12. Time evolution of the instantaneous conversion and particle size during the seeded semibatch polymerization of MMA/BA to produce nanocomposite EP6.

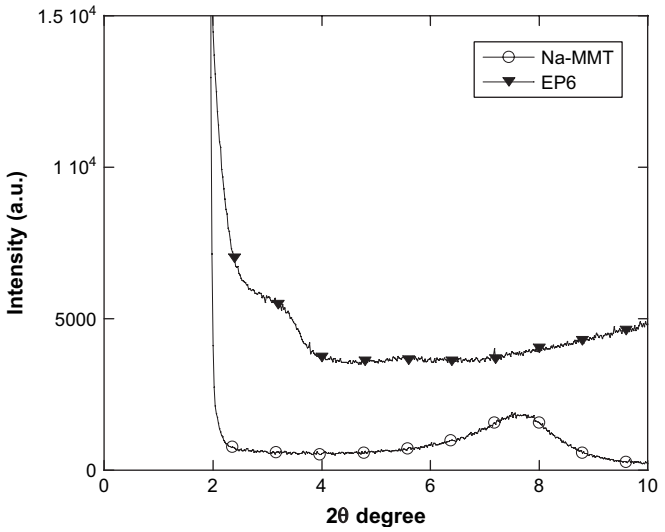

Fig. 13. The WAXD patterns of the nanocomposite film EP6 and of pristine Na-MMT clay.

water, likely because we got rid of the fraction of SLS that migrated to the surface during the film formation [51]. It can be observed that the nanocomposites EP2 and EP3 had a lower WVTR compared with EP1 pure copolymer, due to the "tortuous diffusion path" that retards the progress of the water molecules through the films [50].

3.6. Acrylic/clay waterborne nanocomposites with high solids content

So far all the latexes presented in this work were synthesized with a solids content of 30 wt%. As mentioned in the introduction, in the literature most of the nanocomposite latexes were prepared at most at 20 wt% solids content with few exceptions in which higher solids content waterborne nanocomposites were synthesized [18,52]. However, it is well known that typical formulations used currently in industry to produce coatings and adhesives require higher solids content. Increasing the solids content of waterborne polymer/clay nanocomposites is challenging. On one hand, increasing the solids content while keeping the polymer/clay content constant means increasing the clay/water content, and hence increasing the viscosity of the polymer/clay dispersion in addition to an increase of the number of stacks in the aqueous phase, as shown in the SAXS analysis of Na-MMT dispersions above. Furthermore, the viscosity of aqueous clay dispersion increases quickly with temperature as shown in Fig. 11 and might, therefore, affect the polymerization process which is typically carried out at temperatures above 60 °C. On the other hand, the viscosity of the latex is a function of the volume fraction of the dispersed phase [53] and the presence of the clay platelets ($\approx 200 \times 200 \times 1$ nm) might considerably increase the effective volume fraction for a given solids content, and hence the viscosity of the dispersion. This will increase the particle–particle interaction and consequently make difficult the increase of the solids content without jeopardizing the stability of the latex.

We have attempted to increase the solids content of the formulation presented in Table 1 and to produce waterborne poly(methyl methacrylate-*co*-butyl acrylate)/MMT nanocomposites up to 50 wt% solids content. This meant including all the clay in the initial charge to prepare the seed with 20 wt% solids content (3 wt% clay based on water) and feeding two streams: one with the initiator solution and the second with neat monomer. This strategy worked well up to 40% solids content, however, 50% solids content was not achieved without coagulum formation. Several experiments varying type of initiator and reaction temperature (lower temperatures were attempted with a redox initiator system) led in all the cases to latexes with significant amount of unreacted monomer, extremely high viscosities and coagulum formation for 50% solids content. An operation strategy that worked better and allowed the preparation of a coagulum free acrylic/clay waterborne nanocomposite, EP6, with 45 wt% solids content is presented in Table 2. The main difference between this strategy and the failed attempts was that

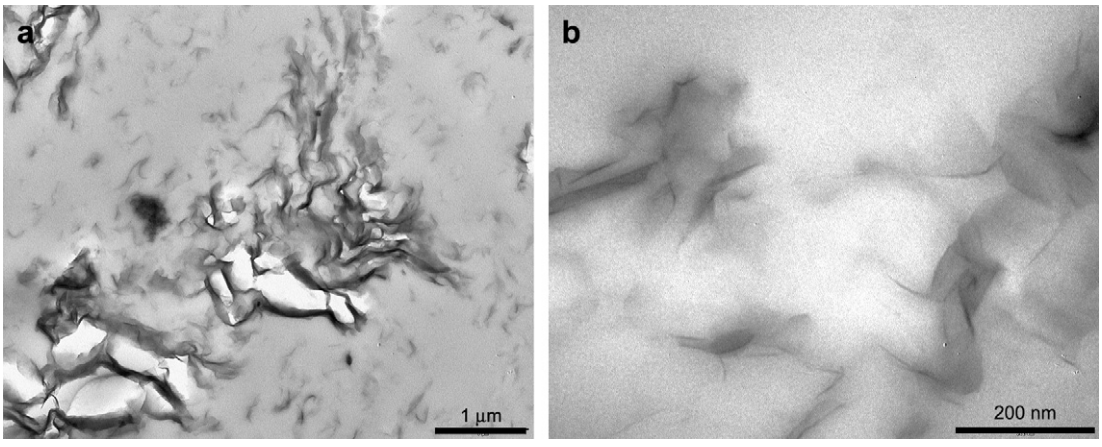

Fig. 14. TEM micrographs of nanocomposite latex film EP6 at different magnifications.

Na-MMT was split between the seed and the feed. This likely allowed to reduce the viscosity of the aqueous phase and the interaction between platelets (because they are at larger distance) and hence to produce stable waterborne nanocomposites.

Fig. 12 displays the evolution of the instantaneous conversion and particle size of this experiment. The instantaneous conversion was high (>92%), i.e., the polymerization proceeded under rather starved conditions. The final particle size was 123 nm and the final viscosity of the latex was 2525 cP (measured in a Viscometer model ELV-8 with spindle number 3 at room temperature).

The WAXD pattern of the nanocomposite EP6 is presented in Fig. 13 and shows an intercalated structure with a broad shoulder at low angles corresponding to a basal distance of 2.76 nm. Fig. 14 presents the TEM micrographs of the nanocomposite EP6 at different magnifications. Individual layers dispersed in the polymer matrix can be observed (see Fig. 14b), but also zones with clay platelet stacks can be distinguished (see Fig. 14a). This is again in agreement with the broad peak at $2\theta = 3.2^{\circ}$ observed in the WAXD pattern. During the seed preparation the aqueous concentration of Na-MMT was lower than 1.5 wt% and hence exfoliated nanocomposite was produced. However, the feed contained Na-MMT at a concentration above 4 wt% in water, and during the particle growth to reach 45 wt% solids content, not all the stacks could be dispersed and hence some aggregates were found in the nanocomposite films.

Table 5 presents the mechanical and thermal properties of the high solids content waterborne nanocomposite latex EP6. As for the low solids content latexes the mechanical properties, tensile strength and storage modulus, clearly improved again at the expense of a decrease in the elongation at break. Glass transition temperature slightly increased (2 °C) without damaging the requirements for a coating application.

4. Conclusions

Waterborne polymer/clay nanocomposite latexes with a mixture of intercalated and exfoliated structures were successfully obtained by *in situ* emulsion polymerization of methyl methacrylate and butyl acrylate with pristine Na-montmorillonite as silicate-layered clay. These nanocomposite latexes presented improved mechanical properties (tensile strength and modulus clearly improved although elongation at break was lower), almost no change in glass transition temperature and reduced water vapor permeability. Waterborne composites can also be prepared by blending a pristine latex with Na-MMT clay. In this work we have shown that composites prepared by the latter method compared well with *in situ* produced waterborne nanocomposites in mechanical and barrier properties, except for the elongation at break that is more affected in the blend (53% reduction as compared with 17%). TEM and XRD demonstrated that the dispersion of the clay is worse for the physical blend. The decomposition temperature is enhanced for both nanocomposites, but the increase for the blend is modest compared with the nanocomposites prepared *in situ*. By considering the additional mixing equipment required to produce this blend, it can be concluded that the *in situ* emulsion polymerization method is advantageous. It has also been demonstrated that increasing the solids content of waterborne nanocomposites is not straightforward. An approach where the clay was split between the seed and the monomer feeding allowed the preparation of poly(methyl methacrylate-*co*-butyl acrylate)/MMT nanocomposite latex with 45 wt% solids content and 3 wt% of clay with intercalated structure and enhanced mechanical properties.

Acknowledgement

G. Diaconu acknowledges the Marie Curie fellowship (HPMT-CT-2001-00227). Financial support by the *Ministerio de Educacion y Ciencia* of Spain (MAT 2003-01963 and Consolider CTQ2006-03412/PPQ), *Basque Government* (ETORTEK 2005) and *European Union* (Napoleon project IP 011844-2) is gratefully acknowledged. The authors want to thank to Dr. Francois Fauth and Dr. Ana Labrador for the SAXS measurements at the Spanish CRG beamline at the European Synchrotron Radiation Facility in Grenoble.

Appendix. Supplementary data

Supplementary data associated with this article can be found, in the online version, at doi:10.1016/j.polymer.2008.03.038.

References

[1] Delair T. In: Daniel JC, Pichot C, editors. Les latex synthetique elaboration, proprietes, applications. Paris: Lavoisier; 2006. p. 699–718.
[2] Urban D, Schuler B, Schmidt-Thünues J. In: Alex van Herk V, editor. Chemistry and technology of emulsion polymerization. Oxford: Blackwell Publishing Ltd.; 2003. p. 226–56.
[3] Tjong SC. Materials Science and Engineering R Reports 2006;53:73.
[4] Tjong SC, Meng YZ. Journal of Polymer Science, Part B: Polymer Physics 2003;41:1476.
[5] Biswas M, Ray SS. Advances in Polymer Science 2001;155:167.
[6] Okada A, Usuki A. Macromolecular Materials and Engineering 2006;291:1449.
[7] Diaconu G, Asua JM, Paulis M, Leiza JR. Macromolecular Symposia 2007;259:305.
[8] Diaconu G, Paulis M, Leiza JR. Macromolecular Reaction Engineering 2008;2:80.
[9] Sun Q, Deng Y, Wang ZL. Macromolecular Materials and Engineering 2004;289:288.
[10] Lee DC, Jang LW. Journal of Applied Polymer Science 1996;61:1117.
[11] Noh MH, Lee DC. Journal of Applied Polymer Science 1999;74:2811.
[12] Noh MH, Jang LW, Lee DC. Journal of Applied Polymer Science 1999;74:179.
[13] Noh MW, Lee DC. Polymer Bulletin 1999;42:619.
[14] Bandyopadhyay S, Giannelis EP. Polymer Material Science and Engineering 2000;82:208.
[15] Zhang Z, Zhao N, Wei W, Wu D, Sun Y. Studies in surface science and catalysis, vol. 156; 2005. p. 529.
[16] Choi YS, Choi MH, Wang KH, Kim SO, Kim YK, Chung IJ. Macromolecules 2001;34:8978.
[17] Choi YS, Wang KH, Xu MZ, Chung IJ. Chemistry of Materials 2002;14:2936.
[18] Li H, Yang Y, Yu YZ. Journal of Adhesion Science and Technology 2004;18:1759.
[19] Park BJ, Kim TH, Choi HJ, Lee JH. Journal of Macromolecular Science Part B Physics 2007;46:341.
[20] Choi YS, Xu MZ, Chung IJ. Polymer 2005;46:531.
[21] Huang X, Brittain WJ. Macromolecules 2001;34:3255.
[22] Meneghetti P, Qutubuddin S. Langmuir 2004;20:3424.
[23] Yeh JM, Liou SJ, Lai MC, Chang YW, Huang CY, Chen CP, et al. Journal of Applied Polymer Science 2004;94:1936.
[24] Herrera NN, Persoz S, Putaux JL, David L, Bourgeat-Lami E. Journal of Nanoscience and Nanotechnology 2006;6:42.
[25] Negrete-Herrera N, Putaux JL, David L, Bourgeat-Lami E. Macromolecules 2006;39:9177.
[26] Li H, Yu YZ, Yang YK. European Polymer Journal 2005;41:2016.
[27] Min HL, Wang JH, Hui H, Jie W. Journal of Macromolecular Science Part B Physics 2006;45:623.
[28] Park BJ, Choi HJ. Science and Technology of Hybrid Materials 2006;111:187.
[29] Lau W. Macromolecular Symposia 2002;182:283.
[30] Cauvin S, Colver PJ, Bon SAF. Macromolecules 2005;38:7887.
[31] Voorn DJ, Ming W, van Herk A. Macromolecules 2006;39:2137.
[32] Miguel O, Fernandez-Berridi MJ, Iruin JJ. Journal of Applied Polymer Science 1997;64:1849.
[33] Van Olphen H. An introduction to clay colloid chemistry. 2nd ed. Malabar, Florida: Krieger Publishing Company; 1991.
[34] Guinier A, Fournet G. Small angle scattering of X-rays. New York: John Wiley & Sons; 1955. p. 268.
[35] Saunders JM, Goodwind JW, Richardson RM, Vincent B. Journal of Physical Chemistry B 1999;103:9211.
[36] Shang C, Rice JA, Lin JS. Clays and Clay Minerals 2001;49:277.
[37] Shang C, Rice JA. Physical Review E 2001;64:021401.
[38] Shang C, Rice JA, Lin JS. Soil Science Society of America Journal 2002;66:1225.
[39] Ciccariello S, Sobry R. Journal of Applied Crystallography 1999;32:892.
[40] Callaghan I, Ottewill RH. Faraday Discussions of the Chemical Society 1974;57:110.
[41] Chern CS, Lin JJ, Lin Y-L, Lai S-Z. European Polymer Journal 2006;42:1033.
[42] Arzamendi G, Asua JM. Macromolecules 1995;28:7479.
[43] Plessis C, Arzamendi G, Leiza JR, Schoonbrood HAS, Charmot D, Asua JM. Macromolecules 2001;34:5147.
[44] Elizalde O, Leiza JR, Asua JM. Industrial & Engineering Chemistry Research 2004;43:7401.

[45] Gonzalez I, Asua JM, Leiza JR. Polymer 2007;48:2542.
[46] Parouti S, Kammona O, Kiparissides C, Bousquet J. Polymer Reaction Engineering 2003;11:829.
[47] Svergun DI, Koch MHJ. Reports on Progress in Physics 2003;66:1735.
[48] Yeom EH, Kim WN, Kim JK, Lee SS, Park M. Molecular Crystals and Liquid Crystals 2004;425:85/[363].
[49] Beall GW, Tsipursky SJ. In: Al-Malaike S, editor. Chemistry and technology of polymer additives, vol. 15; 1999. p. 266.
[50] Okamoto M. Encyclopedia of nanoscience and nanotechnology, vol. 8; 2004. p. 791.
[51] Aramendia E, Barandiaran MJ, Grade J, Asua JM. Langmuir 2005;21: 1428.
[52] Pan M, Shi X, Li X, Hu H. Journal of Applied Polymer Science 2004;94: 277.
[53] Arevalillo A, do Amaral M, Asua JM. Industrial & Engineering Chemistry Research 2006;45:33280.